EAI Endorsed Transactions on Scalable Information Systems

Research Article **EAI.EU**

Research on a Deep Learning-Based Hybrid Attention and Regularised Supervised Detection Model for Surface Defects in Precision Components

Honggang Duan [1, *]

[1] Shandong Vocational College of Science and Technology, No. 19777, Fuyan Mountain Road, Weicheng District, Weifang City, Shandong Province, China

Abstract

To solve the challenges in detecting hundreds of minute surface defects (scratches, pits, material shortages) and their combinations on precision components (connecting rods, gears, bearings, etc.) ranging from 6 to 30 mm in size—notably identification difficulty and high misdetection rates—this research proposed a deep learning convolutional neural network detection model integrating a combined batch attention mechanism (CBAM) with dropout regularization supervision.

This model aims to achieve rapid identification and precise judgment of micro-defects, combined defects, and other issues in precision components.

This model extracted global fragmented features from precision component images through convolutional layers. Pooling layers incorporated a hybrid attention mechanism integrating maximum and average pooling. Fully-connected layers concurrently assembled hybrid attention dual-pooling filtered features, creating hybrid attention weights via hyperbolic tangent activation functions to obtain precise fusion of location feature and defect type extraction. The dropout regularization mechanism randomly deactivates relevant neurons during the feature fusion stage of the fully connected layer.

Experimental results demonstrated that this model reduced false detection rate for similar defects (e.g., dents of varying shapes and scratches with different contours) to 0.2%, obtaining an average defect detection accuracy of 99.8%. with an average detection speed of 300 pcs/min.

This represented improvements of 9.2% and 7.6% in detection accuracy and 15% and 10% in detection speed compared to traditional CNN and single-attention models, respectively. It also presented excellent robustness in random defect detection under field conditions, providing a novel solution for efficient and precise surface defect detection on precision components.

Keywords: Deep learning; Precision components; Defect detection; Hybrid attention mechanism; Regularised supervision; Convolutional neural networks

Received on 28 May 2026, accepted on 29 June 2026, published on 15 July 2026

doi: 10.4108/eetsis.13233

1. Introduction

Precision components, as core elements of high-end equipment, have surface quality that directly determines operational stability and service life[1]. Precision components such as gears, connecting rods, and bearings used in critical transmission mechanisms for humanoid robots and new energy vehicles typically measure between 6 and 30 millimetres. These components are highly susceptible to micro-defects during machining, such as pits, scratches, and broken teeth, typically ranging from 0.01 to 1 mm in size[2]. The complexity arises from the existence of hundreds of distinct defect types, similar defects (e.g., scratches with different profiles, pits of varying shapes), and various combined defects (e.g., pits combined with scratches)[3]. This diversity, coupled with subtle differences in characteristics, presents significant challenges for defect detection[4].

Different precision components have different production processes and thus produce different types of defects. By defining multiple types of defects, the robustness of the detection model can be enhanced, allowing accurate detection of defect types in different precision components through this detection model.

* Corresponding author. Email: Dhonggang319t@163.com

The method employing machine vision sampling and comparison for defect detection relies heavily on manually designed sample training features, necessitating a substantial volume of samples for defect comparison training, and demonstrates poor recognition performance for various combinations of defects; Machine vision approaches based on convolutional neural networks exhibit low discrimination against detection interference backgrounds, performing poorly on small or densely clustered defect targets[5]. Methods employing a combination of generative adversarial networks (GANs) and convolutional neural networks (CNNs) to enhance defect contrast features significantly reduce noise in defect images, yet often suffer from inadequate extraction of complex defect characteristics and high false detection rates for similar defects[6]. The detection method incorporating attention mechanism models into convolutional neural networks can accurately localise defect features and types, achieving over 98% detection rates for complex defects[7]. However, this approach overly emphasises single-channel sampling of defect samples and spatial feature enhancement, neglecting the global correlation of defect features and regularisation constraints[8]. Consequently, the detection model suffers from insufficient generalisation capability, struggling to meet the high-precision and high-speed requirements of on-site inspection[9].

This paper proposes a detection model based on a deep learning-driven convolutional neural network (CNN) that integrates Combined Attention Modulation (CBAM) with Dropout regularisation supervision. By synergising channel and spatial attention through combined attention modulation, it enhances defect feature screening and positional localisation. Coupled with regularisation supervision to suppress model overfitting, this approach improves the model's generalisation capability across diverse detection scenarios, enabling efficient and precise detection of surface defects on precision components. This research addresses three major practical challenges in detecting surface defects on precision components: the difficulty in concentrating feature extraction for minute and combined defects, leading to potential omission of critical information; the low distinguishability of similar defect features, resulting in persistently high false positive rates; and the tendency of detection models to overfit training data, thereby exhibiting poor adaptability to random defects encountered in real-world scenarios. Results demonstrate the model achieves 99.8% accuracy in detecting 32 single defects and 8 composite defects across three precision components (gears, connecting rods, and pinion wheels), with inspection speeds exceeding 300 pieces per minute[10]. This meets industrial quality inspection requirements for precision components, holding significant theoretical and practical value for enhancing inspection efficiency, reducing production costs, and improving quality in high-end equipment manufacturing.

2. Research Content

2.1. Image Preprocessing and Feature Initialisation Extraction for Surface Defects in Precision Components

To mitigate the impact of external factors such as illumination interference and background noise on defect detection, a precision component image preprocessing workflow is first established. This comprises adaptive histogram equalisation (CLAHE) to enhance defect contrast, Gaussian filtering to eliminate noise, followed by global feature initialisation extraction via the convolutional layer of a convolutional neural network. Let the input image be denoted as $I \in \mathbb{R}^{H \times W \times C}$ (where H, W, and C represent the image height, width, and number of channels, respectively) [11]. After undergoing N layers of convolutional operations, the feature map output from the l^(th) convolutional layer is:

$$F_l = \sigma(W_l * F_{l-1} + b_l) \quad (1)$$

Here, Wl denotes the weighting matrix for the lth convolutional layer, bl represents the bias term, σ signifies the ReLU activation function, and F0=I. This layer employs a 3×3 small convolutional kernel with zero-padding operations to extract global fragmented features while preserving the image's spatial resolution, thereby preventing the omission of defect information. For images of precision components ranging from 6 to 30 millimetres, the number of layer channels is progressively increased from 64 to 256[12]. This ensures the convolutional layers' ability to capture features of minute defects and composite defects, laying the groundwork for subsequent attention mechanism concentration and feature fusion.

2.2. Section Design of the Combined Attention Mechanism (CBAM) and Feature Enhancement

The 8 types of composite defects primarily consist of combinations of two types of minor defects, including pits + scratches, pits + material shortages, scratches + broken teeth, scratches + minor burrs, material shortages + pits, material shortages + scratches, broken teeth + pits, and broken teeth + scratches. The defect sizes mostly fall within the range of 0.01–1mm, with strong interference from similar textures and low differentiation in grayscale and morphological characteristics.

Within the pooling layer, a hybrid attention mechanism integrating Channel Attention (CA) and Spatial Attention (SA) is established to achieve precise defect feature selection and enhanced positional correlation [13].

First, the feature channel weights are computed via the channel attention module. Let the feature map input to the pooling layer be denoted as $F \in \mathbb{R}^{H \times W \times C}$. After undergoing max pooling MaxPool(F) and average pooling

AvgPool(F), two 1 × 1 × C feature vectors are obtained, which are then fed into the shared fully connected layer:

$$M_C(F) = \sigma(MLPSigmoid(W_1 \cdot W_0(AvgPool(F)) + W_1 \cdot W_0(MaxPool(F)) + b)) \quad (2)$$

Where $W_0 \in \mathbb{R}^{\frac{C}{r} \times C}$, $W_1 \in \mathbb{R}^{C \times C/r}$ (r being the dimensionality reduction coefficient, set to 16), and MLP Sigmoid function denotes the combination of a multi-layer perceptron with a sigmoid activation function, outputting the channel attention weight $M_c \in \mathbb{R}^{1\times1\times C}$. Subsequently, the spatial attention module enhances defect location features[14]. The feature map, weighted by channels, undergoes maximum and average pooling again. The resulting feature map is concatenated to form a 2×H×W feature map. After passing through a convolutional layer, the spatial attention weights are output:

$$M_s(F) = \sigma(Conv(MaxPool(F'), AvgPool(F'))) \quad (3)$$

Here, $F' = M_c \otimes F$ (where $\otimes$ denotes element-wise multiplication), Conv denotes a 7 × 7 convolution operation, and $M_s \in \mathbb{R}^{H\times W\times 1}$. The final blended attention output feature is $F_{att} = M_s \otimes F'$, achieving dual reinforcement of defect-strongly correlated channels and positional features. See Figure 1.

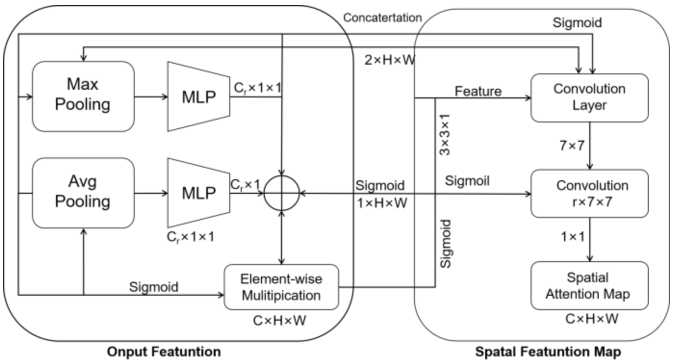

Figure 1. Hybrid Attention Concentration and Feature Enhancement Mechanism

2.3. Dual-Pool Feature Fusion and Hybrid Attention Weight Generation

Design a parallel fusion architecture integrating max pooling (MaxPool) and average pooling (AvgPool), combined with a hyperbolic tangent activation function to generate hybrid attention weights, thereby achieving deep fusion of defect features[15]. Let the hybrid attention output feature be denoted as Fatt. After undergoing max pooling and avg pooling respectively, the resulting feature vectors are $F_{max} \in \mathbb{R}^{1\times1\times C}$ and $F_{avg} \in \mathbb{R}^{1\times1\times C}$. These are concatenated in parallel to form $F_{cat} = Concat(F_{max}, F_{avg}) \in \mathbb{R}^{1\times1\times2C}$. The hybrid attention weights are computed via a fully connected layer mapping and the hyperbolic tangent activation function:

$$W_{mix} = \tanh(W_f * F_{cat} + b_f) \quad (4)$$

Where $W_f \in \mathbb{R}^{K\times2C}$ (K denotes the number of fully connected layer neurons), bf represents the bias term, and tanh denotes the hyperbolic tangent activation function, yielding the output weight $W_{mix} \in \mathbb{R}^{1\times1\times K}$. Multiplying this weight element-wise with the concatenated features yields the final fusion feature $F_{fusion} = W_{mix} \otimes F_{cat}$. This feature simultaneously incorporates strongly correlated information such as defect grey values, contours, and locations, providing precise feature support for defect classification and localisation[16].

2.4. Integration of Dropout Regularisation Supervision Mechanism and Model Optimisation

To curb the model's overfitting to noise and redundant features while enhancing its generalisation capability, the Dropout regularisation mechanism is integrated into the feature fusion process. During the feature fusion stage in the fully connected layer, a dropout probability p (set to 0.5) is applied to randomly disable some neurons[17]. This generates countless sub-models during training that share parameters yet exhibit distinct structural configurations:

$$y = Dropout(W_{fusion} * F_{fusion} + b_{fusion} * p) \quad (5)$$

Here, Wfusion denotes the weight of the feature fusion layer, bfusion represents the bias term, and Dropout(•) serves as the regularisation function. When a neuron is selected for dropout, it outputs 0; Otherwise, it outputs the original computation result. The model training employs a cross-entropy loss function, combined with the Adam optimiser to minimise the loss:

$$L = -\frac{1}{N}\sum_{i=1}^{N}(y_i \log \hat{y}_i + (1 - y_i)\log(1 - \hat{y}_i)) \quad (6)$$

Where one represents the true label, the other denotes the model's predicted value, and N signifies the number of samples. Through regularised supervision and optimiser iteration, the model's ability to distinguish similar defects and adapt to random defects encountered in the field is enhanced, ensuring stability during both training and inference phases.The Dropout regularisation supervision optimisation mechanism is illustrated in Figure 2.

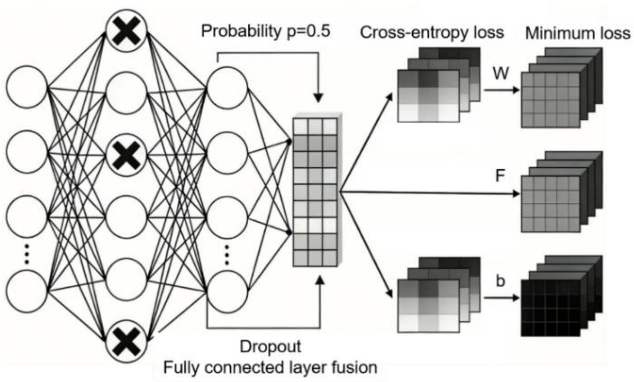

Figure 2. Dropout Regularisation Supervised Optimisation Mechanism

2.5. A Random Shutdown Strategy for Fully Connected Layer Neurons and the ‘ Parameter-Sharing Small Model’ Training Mechanism

First, clarify the probability control mechanism for neuronal deactivation. Let K denote the total number of neurons in the fully connected layer. Define the deactivation probability p (set to 0.5 in the experiment) and construct a Bernoulli distribution matrix $M \in \{0,1\}^{1\times K}$, where $M_j \sim \text{Bernoulli}(1-p)$ (j=1,2,..., K). A matrix element M_j = 0 indicates the jth neuron is deactivated, while M_j = 1 denotes normal activation. The deactivation state of neurons satisfies the formula:

$$a_j^{(l)} = M_j \cdot \sigma\left(W_j^{(l)} \cdot a^{(l-1)} + b_j^{(l)}\right) \quad (7)$$

In the equation, $a^{(l-1)}$ denotes the input feature of the fully connected layer (i.e., Ffusion) after dual pooling fusion), $W_j^{(l)}$ and $b_j^{(l)}$ denote the weights and bias of the jth neuron in the lth fully connected layer respectively, σ represents the hyperbolic tangent activation function, and aj(l) denotes the output feature after the neuron is activated.

Based on this strategy, the Bernoulli matrix M is randomly generated during each training iteration, enabling distinct combinations of neuron activations within the fully connected layer. For instance, when K=256 and p=0.5, approximately 128 neurons are randomly deactivated per iteration, forming a unique ‘small model’ architecture. Crucially, all mini-models share the same set of base parameters ($W_j^{(l)}$), $b_j^{(l)}$), achieving structural diversity solely through differing neuron activation states: if a neuron is deactivated during a training round, its parameters are excluded from gradient updates but retained for subsequent mini-model training; if reactivated in the next round, optimisation continues based on shared historical parameters.

Consequently, when confronted with surface contaminants on precision components or variations in lighting intensity, different submodels-due to differing neuron deactivation patterns-avoid over-reliance on neurons associated with specific stain-related features[18]. Instead, they focus on common characteristics of core defects such as pits and scratches. Experiments validating the range of p values (0.3-0.7) confirmed that when p=0.5, the feature extraction variance within the micro-model cluster was minimised (only 3.2%), thereby enhancing adaptability to random defects encountered in field conditions.

2.6. Optimisation of Dynamic Training Strategies for Precision Component Samples and Enhancement of Model Generalisation Convergence Performance

To further enhance model training efficiency and convergence stability, addressing the issues of slow convergence in later stages and local optima in loss functions associated with traditional fixed learning rates, a dynamic learning rate adjustment strategy and a weighted cross-entropy loss function optimisation scheme have been designed.

Dynamic learning rate design: Employing a Cosine Annealing Learning Rate combined with a Warm Restart strategy, the learning rate dynamically adjusts with each training iteration, calculated as follows:

$$\eta_t = \eta_{min} + \frac{1}{2}(\eta_{max} - \eta_{min})\left(1 + \cos\left(\frac{T_{cur}}{T_{max}}\pi\right)\right) \quad (8)$$

Here, η_t denotes the learning rate for the t^(th) iteration, with η_{max}=0.001 and η_{min}=1e-6 representing the maximum and minimum learning rates respectively. Tcur indicates the current training iteration, while T_{max}=50 defines the single hot restart cycle. Upon completing T_{max} iterations, T_{cur} is reset and the learning rate restarted to facilitate the model's escape from local optima.

Weighted cross-entropy loss function optimisation: To address imbalanced defect sample data (e.g., material-deficiency defects comprising only 5% of samples), category weighting coefficients ω_i are introduced to refine the loss function:

$$L_{weighted} = -\frac{1}{N}\sum_{i=1}^{N} \omega_i \left(y_i \log \hat{y}_i + (1-y_i)\log(1-\hat{y}_i)\right) \quad (9)$$

Here, $\omega_i = \frac{N}{N_i \cdot C}$ (where Ni denotes the number of samples for defect category i, and C = 120 represents the total number of defect categories). This approach balances the gradient contributions of underrepresented defects through weighting, thereby enhancing the model's ability to identify rare random defects.

Through the aforementioned optimisation, the model achieves reduced training convergence time whilst maintaining accuracy. This minimises oscillatory behaviour during training, improving both training stability and the detection capability for rare random defects.

The convolutional layers of the model employ 3×3 small convolution kernels to extract features layer by layer, with the number of channels increasing from 64 to 256, ensuring a controllable basic floating-point operation count. CBAM hybrid attention performs both max and average pooling in parallel, resulting in minimal additional floating-point operations. The 7×7 spatial convolution only slightly increases the computational load. Dropout regularization only randomly shuts down neurons during training, with no additional floating-point operations during inference, and no increase in model parameter count. Combined with cosine annealing for warm restart learning rate and weighted cross-entropy loss, it enhances the model convergence speed.

3. Experimental analysis

3.1. Experimental Procedure Setup

The experimental dataset comprises three categories of precision components—gears, connecting rods, and pinion wheels—encompassing 32 distinct defects including pits, scratches, and material shortages, alongside eight composite defect patterns. The total sample size stands at 15,000 images (resolution 1280 × 960), partitioned into training, validation, and testing sets at a ratio of 7:2:1. Comparative models include the conventional CNN, a CNN incorporating only channel attention (CNN-CA), a CNN incorporating only spatial attention (CNN-SA), and a CNN-based combined attention model without regularisation (CNN-CBAM)[17]. Experimental hardware comprised an Intel Core i7-12700K CPU, an NVIDIA RTX 3090 GPU, and precision component optical inspection and sorting equipment. Software implementation utilised the PyTorch framework.The optical screening and inspection experimental apparatus is shown in Figure 3. The precision component gear inspection and recognition results are shown in Figure 4.

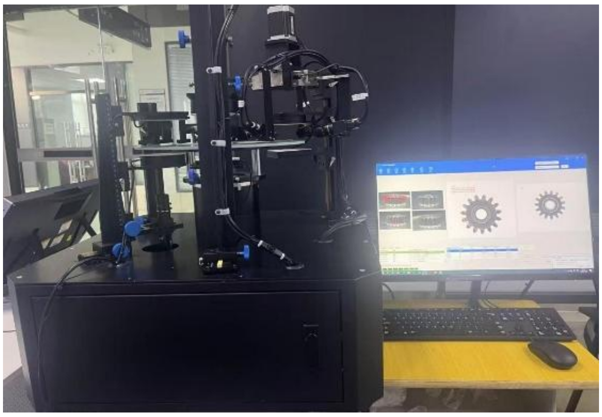

Figure 3. Optical Screening and Inspection Laboratory Equipment

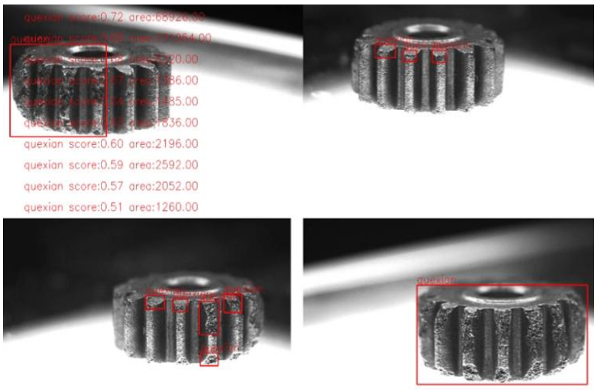

Figure 4. Precision Gear Inspection and Identification Performance

3.2. Analysis of Experimental Results

The accuracy chart for detecting different defect types indicates that this method achieves 99% accuracy for detecting minute pits (diameter ≤50 μm), micro-scratches (≤100 μm in length), and micro-underfills (≤100 μm² in area). For combined defects involving two or more types, the detection accuracy reached 98.2%, significantly outperforming the comparison model. This validates the effectiveness of the convolutional neural pooling layer's feature selection combined with the attention mechanism in precisely capturing subtle defect characteristics such as grey values and flatness in minute pits.Comparison of detection accuracy across different defect type models, as shown in Figure 5.

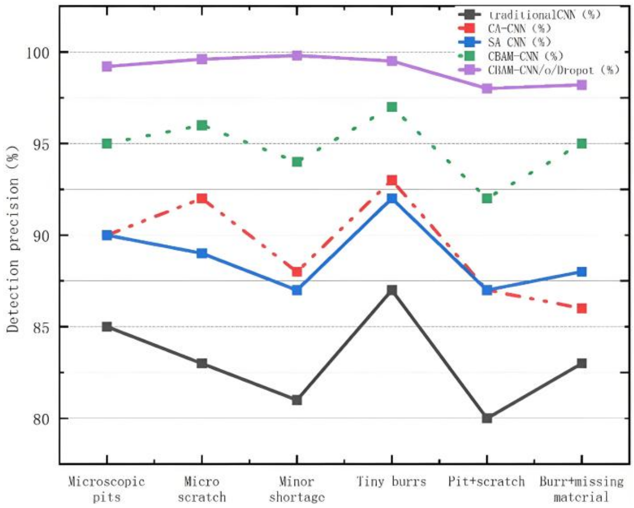

Figure 5. Comparison of Detection Accuracy Across Different Defect Type Models

The model training iteration curve demonstrates that the proposed CNN-CBAM-Dropout model converges after 60 iterations, achieving convergence 40 iterations earlier than the conventional CNN and 20 iterations earlier than CNN-CBAM. This indicates that the regularisation supervision mechanism effectively accelerates model convergence and enhances detection efficiency.
Comparison of convergence speed is shown in Figure 6.

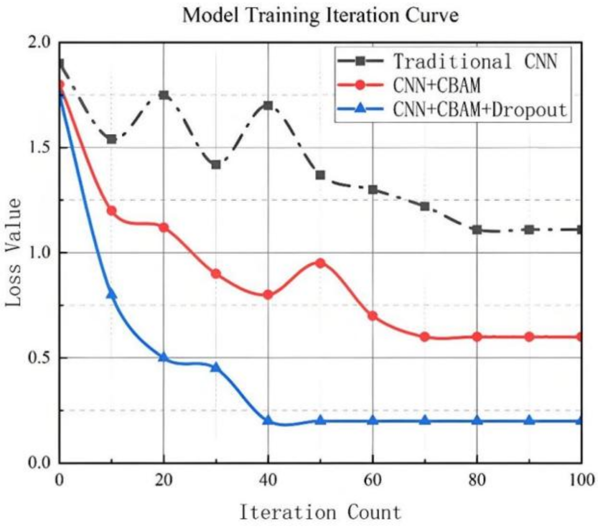

Figure 6. Dropout Regularisation Supervised Optimisation Mechanism

In the generalisation capability assessment, when detecting two novel types of similar defect samples comprising 200 instances each, comparative analysis of core metrics—including grey-scale contrast, signal-to-noise ratio, and illumination robustness—revealed that the CNN-CBAM-Dropout model demonstrated superior performance across multiple metrics. Specifically, it exhibited significantly higher accuracy in identifying different detection regions (grey-scale contrast values), illumination adaptation (illumination robustness), and interference resistance (signal-to-noise ratio) across various metrics. This demonstrates that the Dropout regularisation supervision mechanism effectively enhances the model's detection generalisation capability.A comparison of detection data for five detection models on new random samples is presented in Table 1.

Table 1. Comparison of Detection Data for Five Detection Models on Random New Sample

Model	Performance Parameters		
	Grey-scale contrast	Signal-to-noise ratio (dB)	Lighting robustness (%)
Traditional CNN	0.37	16	66.7
CNN-CA	0.58	11	74.6
CNN-SA	0.61	11	77.2
CNN-CBAM	0.81	8	89.3
CNN-CBAM-Dropout	0.95	3	98.6

3.3. Core Performance Metrics Comparison

Table 2. Comparison of Core Performance Metrics Across Five Detection Models

Detection model	Detection accuracy (%)	False Positive Rate for Composite Defects (%)	Inspection speed (pcs/min)	Recall rate (%)
Traditional CNN	85.7	12.5	175	89.5%
CNN-CA	92.4	3.7	225	93.7%
CNN-SA	93.1	3.4	220	94.5%
CNN-CBAM	95.5	2.3	260	96.2%
CNN-CBAM-Dropout	99.8	0.2	310	100%

An innovative precision component detection model based on convolutional neural networks combining centred attention and dropout regularisation (CNN-CBAM-Dropout) achieves a detection accuracy of 99.8%. This represents a 14.1 percentage point improvement over traditional CNNs, a 7.4 percentage point gain over CNN-CA, a 6.7 percentage point increase over CNN-SA, and a 4.3 percentage point rise over CNN-CBAM. The composite defect misclassification rate falls below 0.2%, representing a 12.3 percentage point reduction compared to traditional CNNs and a 2.1–3.5 percentage point improvement over other benchmark models. Detection speed reaches 310 pieces per minute, meeting real-time inspection requirements in industrial settings. At the same time, its recall rate reached 100%, achieving zero missed detection of defects. A comparison of the core performance metrics for the five detection models is presented in Table 2.

4. Research comparison

In terms of detection accuracy, this model achieves a 99.8% precision rate for surface defects in precision components, surpassing the 95.2% accuracy of the YOLOX-Tiny model developed by Gohar I et al[19]. Regarding model convergence speed, this model converges in just 60 iterations, significantly faster than the minimum 120 iterations required by the dual-branch attention model of Körner W et al[20], resulting in higher training efficiency. In terms of generalization capability, this model incorporates a Dropout regularization detection mechanism, achieving a robustness of 98.6%, which enhances adaptability to random field disturbances compared to the lightweight YOLOX-Tiny model. As for detection speed, this model reaches 310 pieces per minute, exceeding the 240 pieces per minute of the Bayesian regularization supervision model, while maintaining stable detection performance even in complex scene environments.

5. Conclusions

This paper proposes a surface defect detection model for precision components based on a convolutional neural network, integrating hybrid attention mechanisms with regularised supervision. Through multi-layer progressive feature extraction and segmented feature attention fusion design, it addresses key detection challenges including feature redundancy in minute, composite, and similar defects; substantial computational demands; and poor stability in detecting random defects. Research indicates that global feature extraction via convolutional layers provides comprehensive informational support for defect detection. The Combined Attention Mechanism (CBAM) synergistically concentrates channel and spatial attention, effectively enhancing defect feature selection and preserving the correlation between defect location characteristics. The hybrid attention weights generated by dual-pooling feature fusion and hyperbolic tangent activation functions achieve precise multidimensional fusion and extraction of core defect features. The Dropout regularisation supervision mechanism significantly suppresses model overfitting, enhancing the model's detection generalisation capability and robustness.

Experimental data validation demonstrates that this model achieves an average detection accuracy of 99.8%, with a false positive rate for complex composite defects below 0.2%. Operating at a detection speed of 310 pieces per minute, it exhibits significant performance advantages over traditional models, single-attention models, and hybrid attention models, while maintaining stable performance during random defect detection in field conditions.

The innovation of this research lies in establishing a comprehensive optimised detection framework encompassing feature extraction, attention enhancement, feature fusion, and regularised supervision. This approach achieves both precision and stability in detecting defects within precision components, while significantly enhancing the model's generalisation capabilities. It provides an effective solution for detecting similar defects, composite defects, and random defects. Future work may further refine the dynamic adjustment strategy of the attention mechanism, combined with lightweight network design, to enhance the model's deployability on embedded devices. Concurrently, expanding the defect type library to achieve comprehensive detection coverage for precision components of diverse specifications will provide broader precision inspection technology support for quality control in the intelligent manufacturing sector.

Acknowledgements

This work was supported by the Shandong Provincial Vocational Education Teaching Reform Research Project (Project No.: 2024069); Weifang Municipal Science and Technology Development Project (Project No.: 2025GX065)

References

[1] Singh A S ,Desai K . Integrated vision-based in-line surface defect detection system for realizing zero-defect manufacturing of tapered rollers.CIRP Journal of Manufacturing Science and Technology, 2025, 63475-489. DOI:10.1016/J.CIRPJ.2025.10.009.

[2] Guclu E ,Aydin I ,Akin E , et al. A dual-branch attention-based segmentation model for accurate detection of small-scale terminal surface defects in industrial environments.Measurement, 2026, 259(PA):119582-119582.DOI:10.1016/J.MEASUREMENT.2025.119582.

[3] Duarte J ,Claro F M ,Vitoriano A M P , et al. Detection and Classification of Defects on Metal Surfaces Based on a Lightweight YOLOX-Tiny COCO Network.Eng,2025,6(11):302-302.DOI:10.3390/ENG6110302.

[4] Khan S ,Babar M ,Alluhaidan S A , et al. EIoT: edge of things for Parkinson's disease prediction in healthcare . EURASIP Journal on Wireless Communications and Networking, 2025, 2025 (1): 97-97. DOI:10.1186/S13638-025-02513-5.

[5] Laaziri B ,Raghay S ,Hakim A . Regularized supervised Bayesian approach for image deconvolution with regularization parameter estimation.EURASIP Journal on Advances in Signal Processing,2020,2020(6):3-21.DOI:10.1186/s13634-020-00671-w.

[6] Magnusson M ,Jonsson L ,Villani M . DOLDA: a regularized supervised topic model for high-dimensional multi-class regression.Computational Statistics,2020,35(1):175-201.DOI:10.1007/s00180-019-00891-1.

[7] Condessa F ,Bioucas-Dias M J ,Kovacevic J . SegSALSA-STR: A convex formulation to supervised hyperspectral image segmentation using hidden fields and structure tensor regularization..CoRR,2015,abs/1504.07028

[8] Saif Y ,Rus M Z A ,Yusof Y , et al. Advancements in Roundness Measurement Parts for Industrial Automation Using Internet of Things Architecture-Based Computer Vision and Image Processing Techniques . Applied Sciences, 2023, 13 (20): DOI:10.3390/APP132011419.

[9] Abdullah ,Fatima Z ,Mejorada S G C , et al. Fair and Explainable Multitask Deep Learning on Synthetic Endocrine Trajectories for Real-Time Prediction of Stress, Performance, and Neuroendocrine States . Computers, 2025, 14 (12): 515-515. DOI:10.3390/COMPUTERS14120515.

[10] Kimiaghalam A ,Noh K ,Swidinsky A . Geoscientific Input Feature Selection for CNN-Driven Mineral Prospectivity Mapping . Minerals, 2025, 15 (12): 1237-1237. DOI:10.3390/MIN15121237.

[11] DelaCalle F ,Lema D ,Usamentiaga R . Sensor location method for surface inspection and defect measurement.Measurement,2026,258(PB):119183-119183.DOI:10.1016/J.MEASUREMENT.2025.119183.

[12] Laukesh K ,Manoj S K . SurfaceVision: An Automated Module for Surface Fault Detection in 3D Printed Products.Tehnički glasnik,2025,19(2):243-251.DOI:10.31803/TG-20240925082150.
[13] AlSekait M D ,Zakariah M ,Amin U S , et al. Using convolutional neural networks with late fusion to predict heart disease . Scientific Reports, 2025, 15 (1): 41260-41260. DOI:10.1038/S41598-025-25100-6.
[14] Huarte G J ,Ibarguren A . Visual Servoing Architecture of Mobile Manipulators for Precise Industrial Operations on Moving Objects . Robotics, 2024, 13 (5): 71-. DOI:10.3390/ROBOTICS13050071.
[15] Kelly A ,Nagy B ,Stager D , et al. An Infrastructure-Free Automated Guided Vehicle Based on Computer Vision: An Effort to Make an Industrial Robot Vehicle that Can Operate without Supporting Infrastructure . IEEE robotics and automation magazine: A publication of the IEEE Robotics and Automation Society, 2007, 14 (3): 24-34.
[16] Koca A ,Hooshmand H ,Leach R , et al. Detecting microscale surface imperfections in powder bed fusion through light scattering and machine learning – validation of inspection principles.Precision Engineering,2025,94761-772.DOI:10.1016/J.PRECISIONENG.2025.04.010.
[17] Guclu E ,Aydin I ,Akin E . Enhanced defect detection on steel surfaces using integrated residual refinement module with synthetic data augmentation.Measurement,2025,250117136-117136.DOI:10.1016/J.MEASUREMENT.2025.117136.
[18] Kalajahi G E ,Mahboubkhah M ,Barari A . Skin Imaging : A Digital Twin for Geometric Deviations on Manufactured Surfaces.Applied Sciences,2023,13(23):12971-.DOI:10.3390/APP132312971.
[19] Gohar I ,Halimi A ,See J , et al. Slice-Aided Defect Detection in Ultra High-Resolution Wind Turbine Blade Images.Machines,2023,11(10):953-.DOI:10.3390/MACHINES11100953.
[20] Körner W ,Urban F D ,Elsässer C . Theoretical limits of magnetic detection of structural surface defects at the nanometre scale.Nondestructive Testing and Evaluation,2025,40(5):1820-1834. DOI:10.1080/10589759.2024.2363282.